Modular Kirigami Arrays for Distributed Actuation Systems in Adaptive Optics

A.E.M. Schmerbauch,[1,*] A.O. Krushynska,[2] A.I. Vakis,[2] and B. Jayawardhana[1]

[1] *Engineering and Technology Institute Groningen – Discrete Technology and Production Automation, Faculty of Science and Engineering, University of Groningen, Nijenborgh 4, Groningen 9747AG, Netherlands*

[2] *Engineering and Technology Institute Groningen – Computational Mechanical and Materials Engineering, Faculty of Science and Engineering, University of Groningen, Nijenborgh 4, Groningen 9747AG, Netherlands*

(Received 14 September 2021; revised 11 February 2022; accepted 8 March 2022; published 6 April 2022)

The demands on adaptive optics are increasing to achieve high performance and meet the requirements for accuracy and reliability with these systems. At present, common technologies for actuator arrays are highly developed and designed in complex arrangements leading to bulky devices. In this work, we propose an approach for designing modular actuation arrays by means of kirigami metasheets realigned in parallel and leveled in plane. The study focuses on the numerical analysis of different cut patterns to couple lift-off motions within a thin, scalable sheet. A design of a modular actuation array is explained and illustrated in the context of a deformable mirror. The optimal lift-off positions within the array are calculated for this example by a proposed positioning algorithm, which makes use of common methods in adaptive optics such as Zernike polynomial fitting. The algorithm is validated by several simulations calculating the membrane deflection, and the overall concept is discussed.

DOI: 10.1103/PhysRevApplied.17.044012

I. INTRODUCTION

Many engineering developments benefit from advanced structures with tunable material properties, reconfigurable shapes, and versatile functions whose fundamentals are based on origami and kirigami techniques [1–3]. Years ago, the link between optical systems and origami was already established when the reverse corner fold, one of the most popular origami folds, was used for describing optical layouts and simulations of optical systems [4]. Meanwhile, topologies and shapes can be designed by folding and cutting surfaces [5], which has led to inventions such as ultralow-cost foldable microscopes [6], deployable solar panels [7], and inflatable booms for space structures [8,9]. The field of optomechanics is rapidly developing [10]. Besides optomechanical concepts for sensing of mechanical motion [11,12] and fundamental arrays and circuits with higher modes [13,14], actuated systems inspired by kirigami such as microscanners [15], nanokirigami metasurfaces and metastructures for visible light manipulation and reconfigurable optical devices [16,17] were proposed.

Adaptive optics is an advanced technique for optimizing optical systems by correcting the effects of an incoming wave front and its added distortion. Such a technology applies, next to a wave-front sensor and computing system, an active optical element such as a deformable mirror within an imaging system to measure the optical distortion, extract the information and correct the wave fronts by shaping the mirror's surface to redirect the light. These mirrors became an indispensable element of high-performance optical systems and have to meet extreme design and performance requirements such as high spatial resolution, smaller actuator pitch and high-density actuation arrays [18]. However, fulfilling these requirements leads to complicated systems with bulk electronics and huge installation footprints, which become especially challenging, for example, with space-based instrumentation. The design project of the Large Ultraviolet Optical Infrared Surveyor (LUVOIR) [19] and the initial development of a hysteretic deformable mirror [20] have shown the demanding aspects in designing active elements for achieving stable wave-front correction over long periods of time (approximately 10 min) with picometer accuracy [21] for direct exoplanet search and observations. Therefore, lightweight, scalable, and creative solutions are needed to open up further possibilities for the design of such devices and realize the high demands. Various actuator technologies are commonly used, which include, for example, piezoelectric [22–24], electrostatic [25], thermal [26,27], magnetorestrictive, and shape-memory alloy actuators [28], as well as voice coil and reluctance actuators [18,29]. Other approaches can be implemented by metamaterials, which are artificially designed materials with properties usually not occurring in nature [30,31]. Considering mechanical metamaterials, whose main advantages here are scale-invariant mechanical behavior and reversible

*a.e.m.schmerbauch@rug.nl

movements [32], some actuator technologies are based on lightweight, scalable, and simple designs including kirigami cut patterns that lead to buckling-induced three-dimensional (3D) deformations when stretched, and have the potential to be applied in adaptive optical systems. Examples are programmable hierarchical kirigami [33], and kirigami metamaterials with controllable local tilting orientations [34], hybrid cut patterns [35], or multidimensional deformations [36]. Studies that focused on developing controllable actuators by tuning and analyzing cut patterns can be found in the literature [37,38].

In this paper, we propose and numerically analyze kirigami cut patterns for coupling several liftoffs in a thin, scalable metasheet, which enables us to design a modular actuation array that possesses a slim, in-plane design through a conversion of linear displacement into 3D motions. Its application is illustrated in detail by an example of a deformable mirror whose design and positioning of liftoffs are discussed. An algorithm is proposed for placing the cut patterns according to common adaptive optics methods such as Zernike polynomial fitting. The results are presented and the efficiency of the proposed metamaterial array is discussed, while practical guidelines are given.

II. MODULAR ACTUATION ARRAY BASED ON KIRIGAMI

Dias *et al.* [37] recently presented and experimentally evaluated a concept of kirigami actuators whose dynamical pattern formation is controllable based on the arrangement of cuts introduced in a thin sheet. The cuts are functional cracks causing the system to buckle before failure through crack propagation. Therefore, due to a conversion of a linear displacement imposed on the boundary of a thin sheet, it is possible to generate predictable motions. One boundary of the sheet with introduced cuts was clamped while the opposite was subjected to a uniaxial extension perpendicular to the crack. This load condition causes the sheet to buckle in an energetically favorable mode corresponding to predesigned shapes governed by the cuts. Four fundamental modes were elaborated and classified into roll, pitch, yaw, and lift with the out-of-plane displacement occurring at the critical force [37].

Motivated by these results, we propose the design of multiple liftoffs in one kirigami sheet by means on a designed cut coupling for connecting two, three, or more liftoffs in a symmetric arrangement, and numerically analyze them through finite-element nonlinear simulations. In the following, cut couplings for two, three, or more liftoffs in one sheet are referred to as double, triple liftoffs, or metasheets, respectively. The principles of this concept have been validated with the help of proof-of-concept experiments.

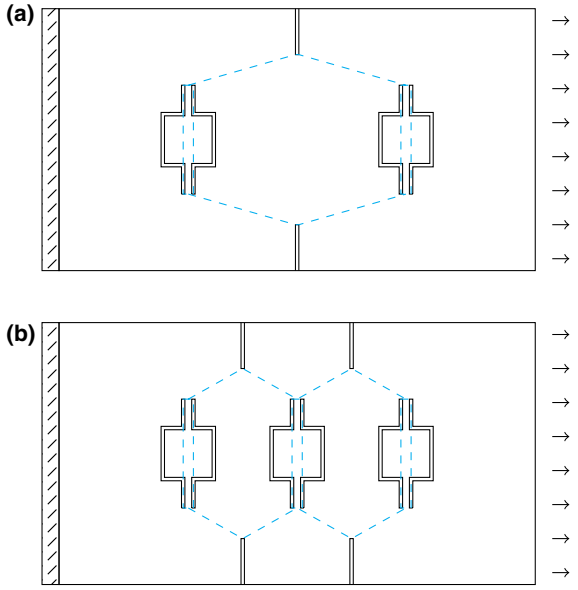

FIG. 1. Cut patterns for a (a) double and (b) triple liftoff (black) generated by rectangular polygons coupled by convex unit cells (blue). The respective sheet is clamped on the left side (section lining) and extended on the right (arrows).

A. Design of cut patterns

To create a double and triple liftoff within one sheet, we need to introduce a separation forming convex polygons, which can be done with two lateral cuts in the middle of the liftoffs. The lateral cuts redirect the tension so that the centers can lift up. A drop of the outer edges at the midline can occur while increasing the extension, but showing only small side effects with smaller out-of-plane displacement. Figure 1 visualizes the cut patterns of double and triple liftoffs. The sheets are clamped on the left side and extended on the right.

B. Numerical validation of cut patterns

The proposed cut couplings are validated numerically by means of finite-element simulations in COMSOL Multiphysics 5.5 using the Structural Mechanics module with the shell interface. The kirigami sheets are modeled in two dimensions (2D) with a thickness of 0.127 mm, length of 182 mm, and width of 100 mm. The material characteristics correspond to Young's modulus of 3.5 GPa and Poisson's ratio of 0.38. The lateral cuts have a length of 20 mm while the central cuts are 40 mm and placed in a distance of 8 mm. The liftoff area amounts to 18×18 mm^2, and is at a distance (center to center) of 80 mm and 40 mm from the adjacent one for the double and triple liftoffs, respectively. One boundary is mechanically clamped while the other has an imposed displacement in regards to the average out-of-plane displacement of the liftoffs to trigger the buckling of the sheet. In addition, the surface

included small, random imperfections (8 orders of magnitude smaller than the sheet thickness) modeled by a parametric surface for simulating the imperfection of the sheet flatness. Nonlinear displacement-controlled stationary analyses are performed to examine the postbuckling behavior of the kirigami sheets.

Figure 2 shows the deformation of the liftoffs in isometric view and visualizes the out-of-plane displacement of the center points of the liftoffs plotted against the uniaxial tension in the metasheet. These results are characterized by a relatively small boundary extension of the kirigami sheet so that the drop of outer edges is comparatively low. It is possible to achieve higher liftoff displacements when the metasheet is optimized in its cut geometry. With increasing lateral cut lengths and concave unit cells, a rotation is initiated. At maximum tension, the lateral cuts take an upright position by flipping during the actuation process. This case is also demonstrated in Fig. 2(c).

The same principles hold for a further extension as long as the arrangement is symmetric. An example of a metasheet with several liftoffs that can be actuated simultaneously is given in Fig. 3.

Based on these results, it is possible to design modular in-plane actuation arrays when single sheets are arranged in parallel and driven distributively by linear motors. This will allow an individual actuation of certain liftoffs and impose the required components in plane. Due to the fact that sheets with different numbers of liftoffs have the same geometrical dimensions, large-scale arrays can be created and adapted to the desired needs. An example of an application in the field of adaptive optics is presented in Sec. III.

C. Proof-of-concept experiments

To validate the feasibility of the cut coupling and show that the behavior of the kirigami actuators is insensitive to scale or material, we perform proof-of-concept experiments. Test samples are manufactured from PVC sheets with a thickness of 0.3 mm using a VEVOR CNC 3018 engraver machine with a 5500-mW laser. The cut geometries are scaled down with a factor of 3.5 to obtain kirigami sheets with a total width of 28 mm and length of 60 mm. The proportions are slightly adjusted to adapt the samples according to the test setup.

The experiments are carried out with an Instron 5944 Universal testing machine with customized clamps for thin sheets. Extension controlled tests are performed at a rate of 0.25 mm/min to a maximum extension of 1.8 mm. We test three samples each for the different cut patterns (double and triple liftoff), and record their deformation with a Panasonic HDC-SD60 Full HD camera. The samples experienced light inelastic strains, but the actuation is reversible. Figure 4 presents the sheets in an isometric view at the maximum extension while Fig. 5 shows the displacements during the experiments from a side view. Videos of the experiments can be found within the Supplemental Material [39].

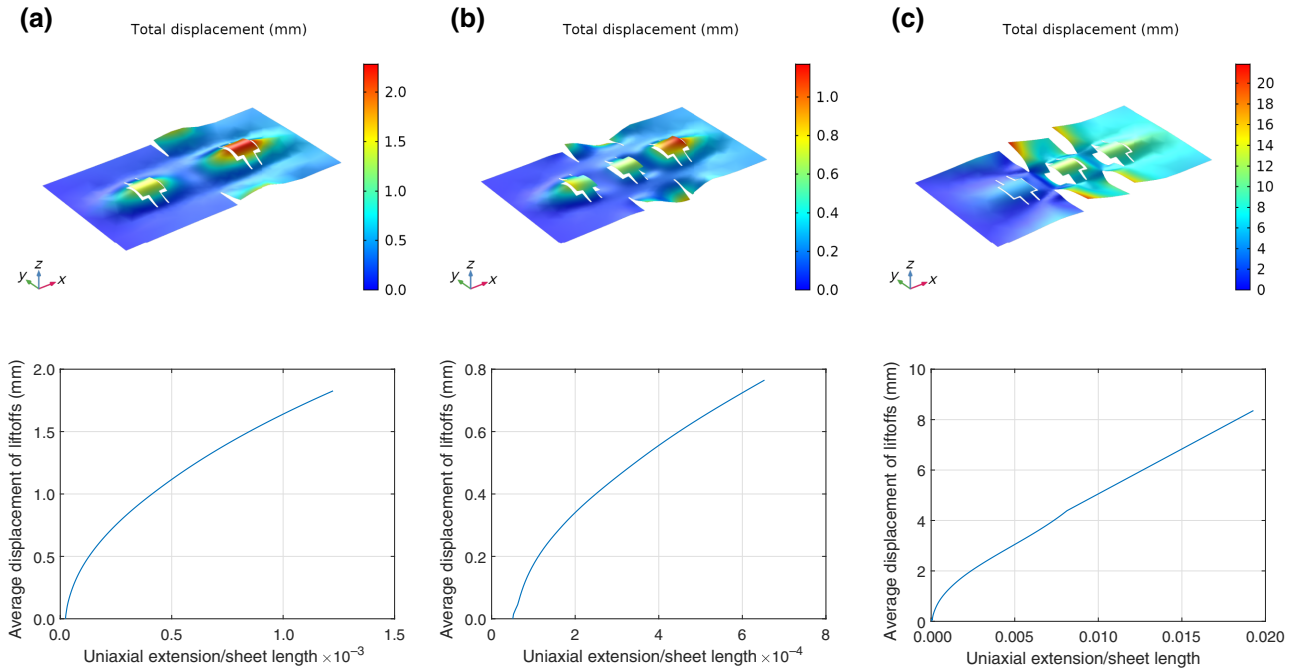

FIG. 2. Out-of-plane displacement in isometric view (top) and average out-of-plane displacement of liftoffs' center plotted against uniaxial extension normalized by sheet length (bottom) for a (a) double liftoff and (b) triple liftoff as well as a triple liftoff with coupled concave unit cells and high displacement is presented in (c).

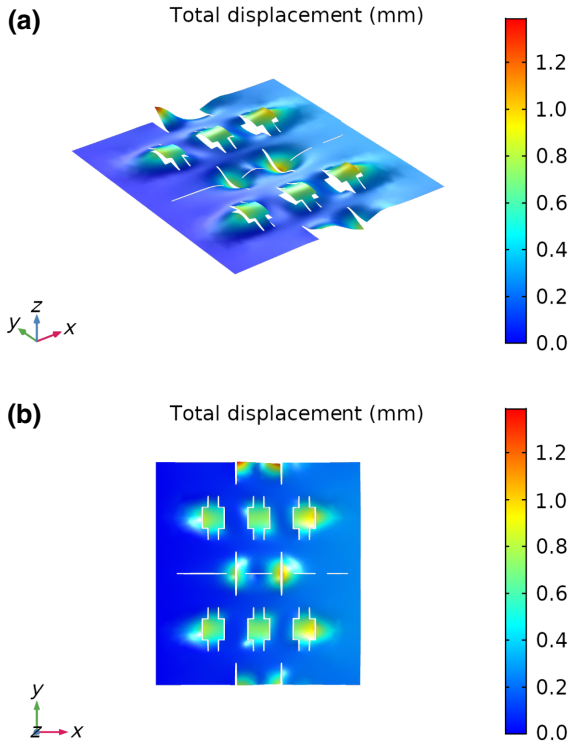

FIG. 3. Metasheet with several cuts exerting six liftoffs during actuation. The actuated sheet is presented in (a) isometric view and (b) top view.

III. APPLICATION OF KIRIGAMI ARRAY IN ADAPTIVE OPTICS

We present a concept for deformable mirrors using the proposed modular kirigami actuation array. The structure is limited to a series of single metasheets mounted in parallel and subjected to a displacement by use of separate linear actuators. Each metasheet contains different cut patterns that couple vertical liftoffs that are purposely designed to create common deformations for light wave-front aberrations as illustrated in Fig. 6. The parallel-arranged metasheets are designed in width and length such that they can cover the active area of the mirror. Beyond a sheet length-to-width ratio of about $L/w \approx 1$, the sheet length does not contribute to the crack deformation [37]. This allows us to flexibly adjust the length of the metasheets for the mounting of the linear actuators. In addition, kirigami actuators are weakly dependent on sheet thickness according to the present analytical model so that also the sheet thickness can be considered as a design parameter. The facesheet of the mirror is placed at a sufficient distance to the metasheets, which can be determined by analyzing liftoff displacements and desired membrane deformation. When the linear motors are actuated, the respective sheet will buckle and change its shape deformation to the encrypted liftoffs that generate a pressure on the mirror facesheet. Because it is not possible to create negative deformations on the membrane, all corrections are normalized to positive. We use the large span of operation of the kirigami actuators to generate the leveling between the actuators above zero. A specific selection of membrane material can also contribute with its stiffness to the mechanical coupling and smoothing between the actuators in the array. This mirror can be designed at the nano-, micro-, or macroscales due to the scale-invariant mechanical behavior of kirigami sheets.

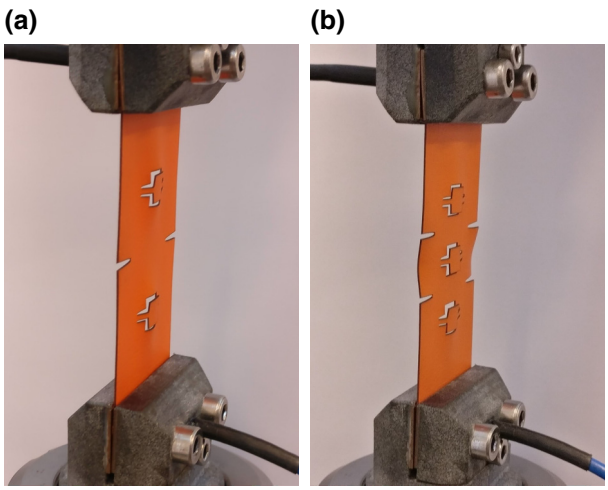

FIG. 4. The extended sheets with a (a) double liftoff and (b) triple liftoff from an isometric perspective.

A. Algorithm for determination of best liftoff positions

The performance of deformable mirrors is evaluated by determining how well the actuators can reproduce a desired surface shape on the reflective membrane. Zernike polynomials are the preferred representation for light wave-front aberrations in adaptive optical systems [40] and are commonly chosen to test the possibilities of the actuator arrays. They are defined on a unit circle as functions of azimuthal frequency p and radial degrees q, where $p \leq q$ using polar coordinates (r, θ). The set of polynomials can be given by

$$\begin{aligned} Z_q^p(r,\theta) &= R_q^p(r)\cos(p\theta) \quad \text{for} \quad p \geq 0, \\ Z_q^{-p}(r,\theta) &= R_q^p(r)\sin(p\theta) \quad \text{for} \quad p < 0, \end{aligned} \tag{1}$$

where

$$R_q^p(r) = \sum_{S=0}^{(q-p)/2} \frac{(-1)^S (q-S)!(r^{q-2S})}{S![(q+p)/2-S]![(q-p)/2-S]!}. \tag{2}$$

The deformed mirror shape in response to the actuation of a single actuator can be calculated by means of plate models and actuator influence functions. In the following, we propose an algorithm for placing the cut patterns according

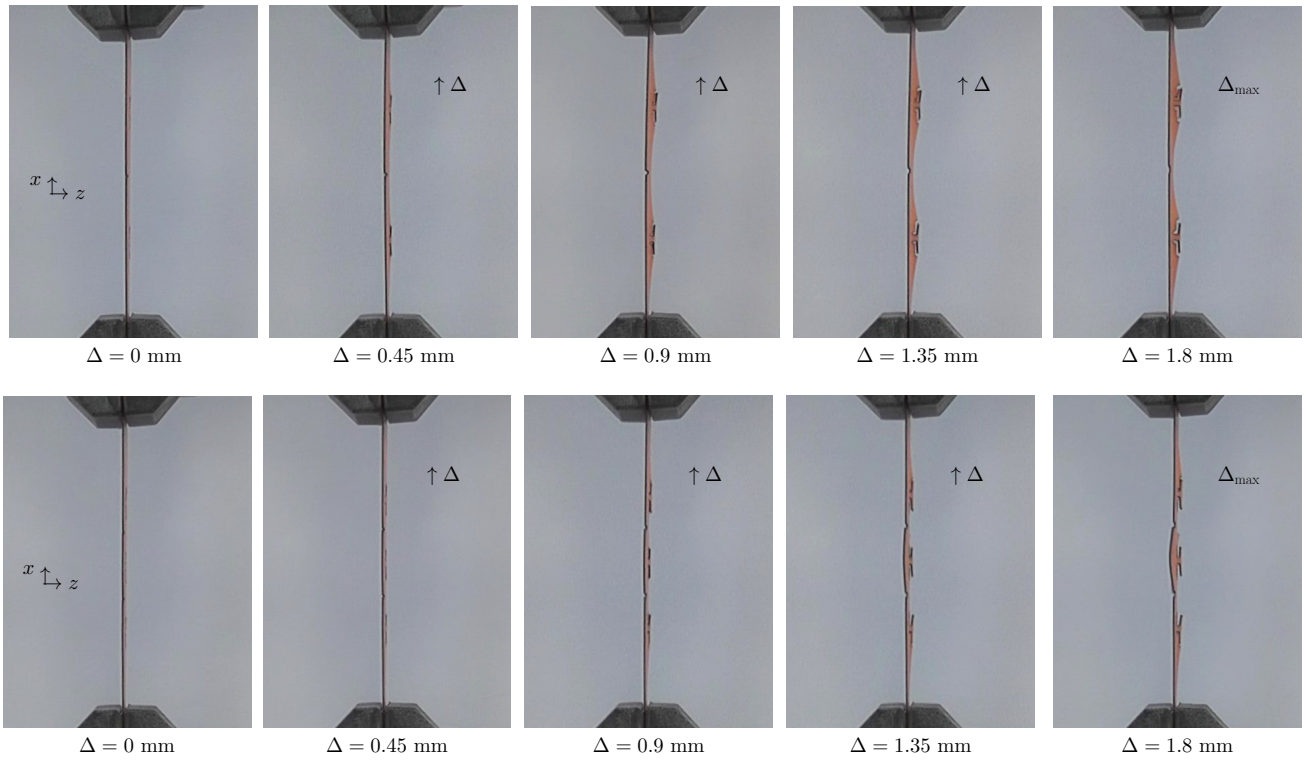

FIG. 5. Proof-of-concept experiments for a sample with double and triple liftoff. The photo series in the top shows the deformation with increasing extension for a double liftoff and the photo series in the bottom presents the triple liftoff.

to selected low-order Zernike polynomials. Based on the influence functions [41], we can identify the optimal positions for every liftoff per sheet by extending it to a reverse method with initial pressure input and no dependency on any input position.

The optimization is done in two steps by means of minimizing the sum of the squares of the residuals made in the results of every single equation. In the first step, we consider the matrix equation from [41] given by

$$\boldsymbol{z} = \mathcal{M}\mathbf{P}, \tag{3}$$

where $\boldsymbol{z}$ denotes the $n \times 1$ vector containing the deflection per surface points, $\mathcal{M}$ the $n \times m$ coefficient matrix, and $\mathbf{P}$ the $m \times 1$ pressure vector. We note that the unknown in this case is the coefficient matrix, which denotes the influence functions per surface point. To perform a least-squares fitting on the matrix $\mathcal{M}$ to identify the optimal position based on the coefficient calculation, we vectorize the matrix $\mathcal{M}$ by stacking the columns of the matrix on top of each other. The vectorized form of $\mathcal{M}$ is denoted by $V^{nm}(M)$ and given by

$$V^{nm}(M) := [a_{11}a_{21}\ldots a_{n1}a_{12}a_{22}\ldots a_{n2}\ldots a_{1m}a_{2m}\ldots a_{nm}]^{\mathsf{T}}. \tag{4}$$

The corresponding coordinates associated to each element in $V^{nm}(M)$ are given by

$$\varepsilon_{n\times m}^{\mathrm{col}} = (E_{11}, E_{21}, \ldots, E_{n1}, E_{12}, E_{22}, \ldots, E_{n2}, \ldots, E_{1m}, E_{2m}, \ldots, E_{nm}). \tag{5}$$

The pressure vector must be n-times repeated and transposed, and can be denoted as P^{T}. For compactness, the vector $V^{nm}(M)$ is denoted as $\mathrm{vec}(M)$ in the following. Using the Kronecker product, matrix multiplication can be expressed as a linear transformation of vectorized matrices. Hence, the first least-squares problem is associated with

$$\mathrm{vec}(z) = \underbrace{(P^{\mathsf{T}} \otimes I)}_{:=K}\mathrm{vec}(M), \tag{6}$$

which can be solved by standard numerical techniques. The system is underdetermined with an infinite number of solutions. We find the smallest solution by minimizing $\mathrm{vec}(M)$ subjected to the constraint $\mathrm{vec}(z) = (P^{\mathsf{T}} \otimes I)\mathrm{vec}(M)$ and solve according to

$$\mathrm{vec}(M) = K^{\mathsf{T}}(KK^{\mathsf{T}})^{-1}z. \tag{7}$$

After the solution $\mathrm{vec}(M)$ is obtained, the vector can be transferred back to the initial coefficient matrix $\mathcal{M}_{ij}$,

which denotes the influence function at surface positions labeled $i = 1, \ldots, N_a$ per jth actuator.

In the second step, we calculate optimal positions of the liftoff based on the obtained coefficients. For this, the formulation of *Case V* from Ref. [41] is rewritten and the radial limits substituted by the center point of the approximate liftoff positions to obtain a nonlinear multivariable function. This function can be given by

$$
\begin{aligned}
f(x) = M_{ij} - \Bigg\{ \Bigg(& \frac{1}{2\pi} \Bigg\{ \Delta\phi_j [-\ln r_i] \left[r_i^2 - \left(x - \frac{p_w}{2} \right)^2 \right] / 2 \\
& - \sum_{n=1}^{\infty} \frac{r_i^2}{n^2 (n+2)} [r_i^{2n} - 1] \times \left[\left(\frac{r_i^2}{r_i} \right)^{n+2} - \left(\frac{(x - \frac{p_w}{2})}{r_i} \right)^{n+2} \right] \\
& \times [\sin n(\phi_{2j} - \phi_i) - \sin n(\phi_{1j} - \phi_i)] \Bigg\} \Bigg) \\
& + \Bigg[\frac{1}{2\pi} \Bigg(\Delta\phi_j \left\{ \left(x + \frac{p_w}{2} \right)^2 \left[\frac{1}{2} - \ln \left(x + \frac{p_w}{2} \right) \right] - r_i^2 \left(\frac{1}{2} - \ln r_i \right) \right\} / 2 \\
& - \sum_{n=1}^{\infty} \frac{1}{n^2} \left\{ r_i^n \left[\left(x + \frac{p_w}{2} \right)^{n+2} - r_i^{n+2} \right] / (n+2) + \alpha \right\} \times [\sin n(\phi_{2j} - \phi_i) - \sin n(\phi_{1j} - \phi_i)] \Bigg) \Bigg] \Bigg\}
\end{aligned}
\tag{8}
$$

where $\Delta\phi_j$ is the approximated liftoff size in the angular coordinate calculated by the subtraction of upper by lower angular limit ϕ_{2j} and ϕ_{1j}; r_i is the radial position on a specified surface point i; x is the center position of the liftoffs; p_w is the liftoffs' width, and α is an additional factor based on the radial limits. The infinite sums are approximated by using a lower limit on series term size (before multiplication by sine term) of 1×10^{-7}.

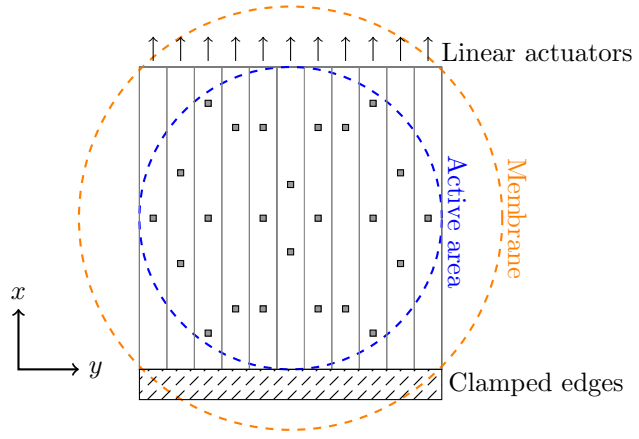

FIG. 6. Conceptual visualization of the deformable mirror based on kirigami actuators shown in a schematic way. The squares illustrate the liftoffs whose position will be optimized by our proposed algorithm. The sheets are arranged next to each other with one edge clamped (illustrated by shading) and the other one extendable using linear actuators (illustrated by arrows) so that the active area of the mirror's membrane is covered.

To enable finding the optimal position for the liftoffs over the length of a single kirigami actuator sheet, we make a preselection of actuator positions relevant to the corresponding Zernike polynomials. For that, we rely on a property of the Zernike polynomials, namely, the rotational symmetry that allows the polynomials to be expressed as products of radial terms and functions of angle, $r(\rho)g(\theta')$. Here $g(\theta')$ is continuous and repeats itself every 2π radians. Based on these symmetries, we determine a certain amount of liftoffs in one sheet (for simplicity, two) for a specific Zernike polynomial from the basis functions presented in Fig. 7.

The preselection of positions is intuition-based and follows the principle of considering the points of highest

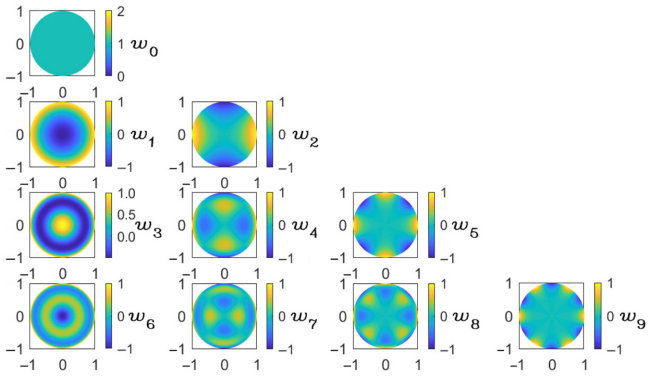

FIG. 7. First ten basis functions selected from Zernike polynomials.

TABLE I. Summary of activated sheets with 11 kirigami actuators in the deformable mirror per selected basis function of the Zernike polynomials (ZPs). A sheet is activated when the pressure ($\hat{P}$) is set, otherwise it is zero.

	Kirigami metasheet										
ZP	1	2	3	4	5	6	7	8	9	10	11
w_1	$\hat{P}$	$\hat{P}$	$\hat{P}$	$\hat{P}$	0	0	0	$\hat{P}$	$\hat{P}$	$\hat{P}$	$\hat{P}$
w_2	$\hat{P}$	0	0	0	0	0	0	0	0	0	$\hat{P}$
w_3	$\hat{P}$	$\hat{P}$	$\hat{P}$	$\hat{P}$	$\hat{P}$	$\hat{P}$	$\hat{P}$	$\hat{P}$	$\hat{P}$	$\hat{P}$	$\hat{P}$
w_4	$\hat{P}$	0	0	0	$\hat{P}$	0	$\hat{P}$	0	0	0	$\hat{P}$
w_5	$\hat{P}$	0	0	$\hat{P}$	0	0	0	$\hat{P}$	0	0	$\hat{P}$
w_6	$\hat{P}$	$\hat{P}$	$\hat{P}$	$\hat{P}$	$\hat{P}$	0	$\hat{P}$	$\hat{P}$	$\hat{P}$	$\hat{P}$	$\hat{P}$
w_7	$\hat{P}$	0	0	$\hat{P}$	$\hat{P}$	0	$\hat{P}$	$\hat{P}$	0	0	$\hat{P}$
w_8	$\hat{P}$	$\hat{P}$	0	$\hat{P}$	0	0	0	$\hat{P}$	0	$\hat{P}$	$\hat{P}$
w_9	$\hat{P}$	0	0	$\hat{P}$	0	0	0	$\hat{P}$	0	0	$\hat{P}$

deformation. Liftoffs can only lie on the horizontal centerline of a sheet. In addition, the vertical distribution for the sheets accordingly follows the first ten basis functions.

Then, we find the minimum of the set of equations involving Eq. (8) by formulating it as a nonlinear least-squares fitting problem that can be denoted by

$$\min_x \|f(x)\|_2^2 = \min_x [f_1(x)^2 + f_2(x)^2 + \cdots + f_n(x)^2] \quad (9)$$

with lower (LB) and upper bounds (UB) on the x component so that the solution is always $\text{LB} \leq x \leq \text{UB}$. The lower bound refers to zero and the upper bound to the value equivalent to the edge of the unit disc at the sheet centerline. Only the right half of the unit disc is considered due to the symmetric arrangement of the liftoffs on a sheet.

The nonlinear least-squares solver (lsqnonlin) of MATLAB [42] starts at the point x_0, which is defined in the most likelihood area based on *a priori* knowledge, and finds a minimum of the sum of squares of the defined vector-valued function defined as

$$f(x) = \begin{bmatrix} f_1(x) \\ f_2(x) \\ \vdots \\ f_n(x) \end{bmatrix}. \quad (10)$$

TABLE II. Summary of the results for a deformable mirror actuated by 11 kirigami actuators with two or three liftoffs each. The optimal positions of every liftoff in regards to the selected ZP are given in the column of x, and are considered as symmetric arrangement on the kirigami sheet.

Sheet	Height centerline	ZP	x_0	x	Quantity
1	10/11	w_5	0	0.4100	1
2	8/11	w_9	0.45	0.6800	2
3	6/11	w_8	0.35	0.7984	2
4	4/11	w_7	0.6	0.9300	2
5	2/11	w_3	0.15	0.2050	2
6	0	w_2	0.85	0.2228	2
7	−2/11	w_3	0.15	0.2050	2
8	−4/11	w_7	0.6	0.9300	2
9	−6/11	w_8	0.35	0.7984	2
10	−8/11	w_9	0.45	0.6800	2
11	−10/11	w_5	0	0.4100	1

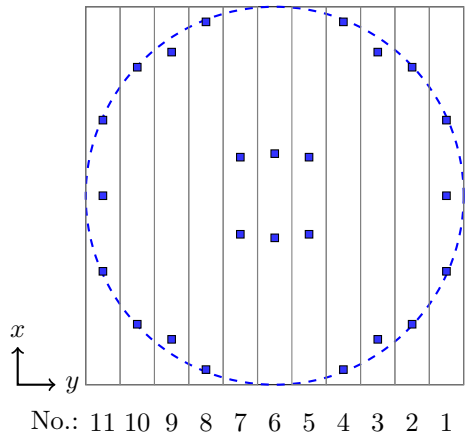

FIG. 8. Deformable mirror with kirigami-based actuation showing the optimal positions of the double and triple liftoffs illustrated as blue squares inside the active area (dashed blue circle).

B. Arrangement of liftoffs

To illustrate the results, we run several MATLAB (MATLAB R2019a) simulations to evaluate the best positions for the liftoffs. Within the concept of a deformable mirror, we actuate 11 kirigami actuators with two liftoffs each. Only

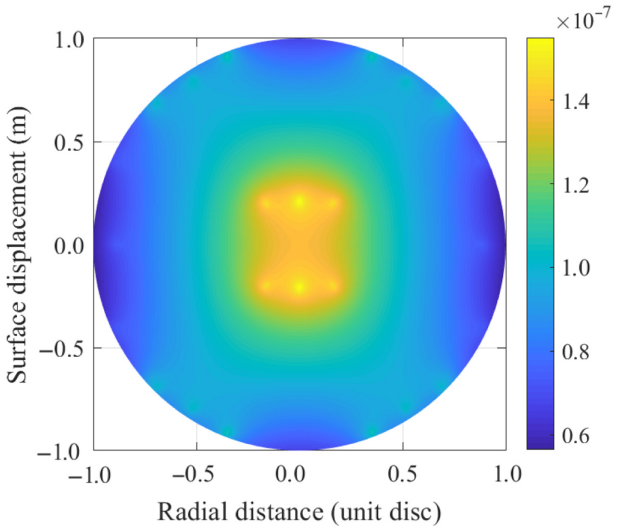

FIG. 9. Surface plot of the mirror membrane (active area) when all liftoffs are activated and exert the same pressure. The vertical colorbar gives the membrane displacement in m.

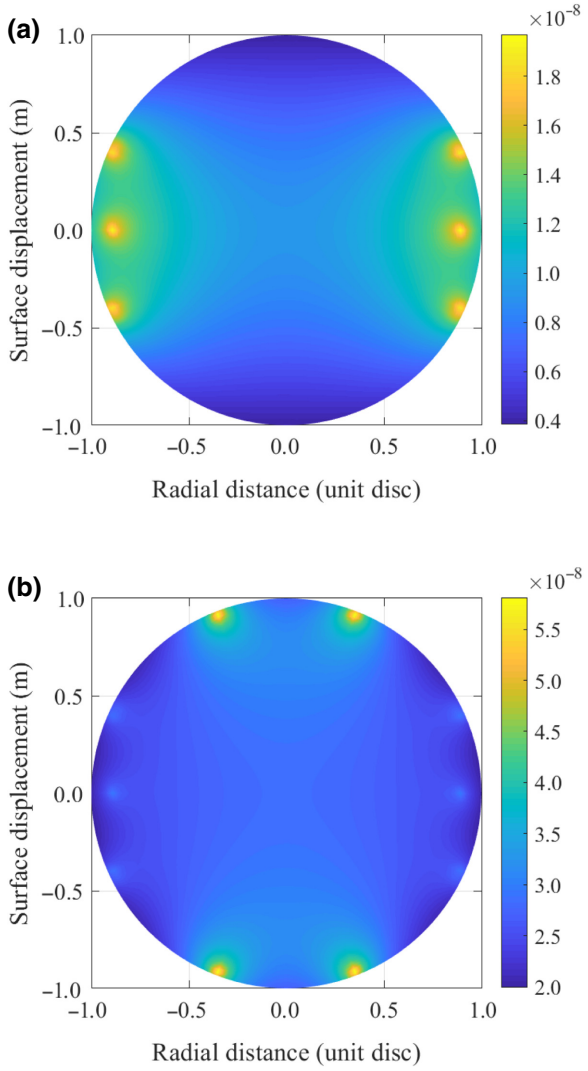

FIG. 10. Surface plot of the mirror membrane (active area) when all liftoffs mentioned in Table II for w_2 (a) and w_5 (b) are activated and exert the same pressure. The vertical colorbar gives the membrane displacement in m.

the outer sheets have a triple liftoff to cover the open edges. The mirror diameter (active area) is normalized to a radius of 1 while the initial dimensions amount to an active area of 50 mm, a membrane diameter of 70 mm, a sheet width of 4.5 mm, and a liftoff size of 1×1 mm^2 with a rather trapezoidal shape due to the plate model. The membrane surface tension is to 15 N/m.

The horizontal distance was restricted to the centerlines of every sheet, which correspond to 10/11, 8/11, 6/11, 4/11, 2/11, 0, $-2/11$, $-4/11$, $-6/11$, $-8/11$, and $-10/11$ considering the arrangement in terms of the unit disc from right to left numbering the sheets from 1 to 11 in ascending order. The surface points are distributed in a squared arrangement to fully cover an area that contains the unit disc. In total, 100 surface points are selected at a horizontal distance of 0.01 per unit disc radius.

The preselection is done by choosing certain kirigami actuators to be responsible for reproducing specific basis functions as summarized in Table I. The initial distribution at x_0 is listed in Table II. The results for the optimized liftoff positions are illustrated in Fig. 8 and further specified in Table II.

Figure 9 presents the active area of the membrane when all liftoffs are activated with a pressure set to 1 N/m for simplicity. The membrane displacement is calculated based on the presented model in Ref. [41]. In addition, Fig. 10 shows the basis function w_2 and w_5 to illustrate the principle of fitting the mirror surface.

IV. DISCUSSION AND CONCLUSIONS

In summary, we design and apply concepts of cut coupling in kirigami actuators and numerically analyze their out-of-plane displacements by finite-element simulations. Proof-of-concept experiments demonstrate the feasibility of the principles and show that the behavior of kirigami actuators is insensitive to scale and material. The liftoff positions in the mechanical metasheets can act as actuators when they are evoked by a linear displacement of the metasheet itself. Based on a parallel arrangement of several kirigami sheets with either double, triple, or multiple liftoffs, modular actuation arrays are generated, which can be applied, for example, in adaptive optics. A concept for a deformable mirror is illustrated in detail and optimized positions for the liftoffs of the actuation array are determined by means of a developed reverse position algorithm. Due to the small number of liftoffs in the example, high surface fitting accuracy cannot be reached. Nevertheless, the number of actuators and thus, the degrees of freedom, can be increased by exploring larger arrays. For example, high-precision performance requires dense actuator arrays. The current state of the art is 64×64 actuators demonstrated by fully functional deformable mirrors of Boston Micromachines Corporation (correction in astronomical imaging instruments) [43] and AOA Xinetics (correction of high-energy and high average power lasers) [44]. To achieve modular arrays with a few thousand liftoff positions, more complex metasheets have to be designed and aligned in such a way that the covering of the active area of the mirror is maximized. It may be advisable to break up the parallel arrangement and position the individual sheets in an optimized way. Due to the large deformations that can be achieved by the liftoff mechanism with optimized cut geometry, the sheets no longer have to be leveled in-plane but in their peak deformation instead, and could also generate asymmetrical patterns when positioned with overlay. However, for the correction of low-order aberrations and other sorts of applications fewer numbers of actuators could be also appropriate.

The proposed system is characterized by a scalable design ranging from nanoscale to macroscale since

the kirigami actuators have a scale-invariant mechanical behavior. Therefore, it has a promising potential for various applications in the field of adaptive optics. The developed modular array presents a lightweight solution since the actuators can be made, in the simplest sense, of paper like traditional kirigami. Nevertheless, additional linear actuators are required to activate individual sheets in a targeted manner. Here, the number of liftoffs chosen must be compared to the number of required linear actuators. Then it can be reflected whether this concept is advantageous for the application-related demands.

Moreover, kirigami structures show relative independence from their base material, which significantly expands the choice of material. By optimizing the cut geometries for different materials, comparable movements can be achieved within the actuation. In addition, the overall arrangement comprises an in-plane design due to the fact that linear displacements are converted to an out-of-plane deformation, which opens up the possibilities for compact and slim layouts for optical systems such as the deformable mirror in space-based applications.

The presented analysis needs to be exploited by investigating and measuring the generated pressure of the liftoffs when the kirigami sheet is operated. This will determine which deformation profiles can be achieved for different membranes and materials. It is also necessary to determine a required distance between an actuation array and a membrane so that the buckling-induced liftoff will always take its favorable state and function in a reliable way.

While we discuss only symmetrical arrangements in the positioning of liftoffs within one sheet and the placement of metasheets for covering the active area of the mirror, asymmetrical cut patterns and arrangements should be explored, which would increase the complexity and lead to more flexibility in designing the modular array. This could eliminate the limiting factor related to the response accuracy for a dynamic input and degrees of freedom.

The preprogrammed behavior of the individual actuators must be well thought out for the application. By means of suitable combinations of encrypted liftoffs, the possibilities can be extended such that a good number of correction elements and liftoffs can be connected to each other. The generation of a tailored control strategy of the mirror linked to the wave-front sensor and computing system is advisable. While the presented concept of actuating the deformable mirror with a modular array contains only one layer of information, in the future it may be possible to encode several layers into one metasheet and then evoke the desired combination of liftoffs in a targeted manner. Research works such as Refs. [33,38,45] show how different layers of information can be textured.

The kirigami sheets can be further optimized and adapted to other specific applications. Based on the proposed idea, this could include, for example, the (static) correction of small misalignments, aberrations, imperfections, or undesired surface textures in other materials. For that, different cut couplings might be useful and instead of pure symmetrical arrangements, other fundamental modes of roll, pitch, or yaw, and their combination could be explored.

In conclusion, the modular kirigami array for distributed actuation systems is characterized by its reliability and robustness since this concept would not suffer from a total failure when a single sheet loses functionality. The array can be upgraded and improved by replacing and changing the corresponding metasheets. The assignment of single functions to individual sheets offers high flexibility in the design. However, this concept is affected by the losses and suboptimal use of space due to the transitions between single kirigami actuators with simple cut coupling and small number of liftoffs. For that reason, the investigation of more complex cut couplings is helpful to advance this actuation system for applications in adaptive optics.

ACKNOWLEDGMENTS

We thank Dr. M. Acuautla, Dr. T. Mokabber, S. Taleb, and Z. Zhang from the Engineering and Technology Institute Groningen for their technical support and the provision of access to the machines for performing the proof-of-concept experiments.

[1] Nicholas Turner, Bill Goodwine, and Mihir Sen, A review of origami applications in mechanical engineering, Proc. Inst. Mechanical Eng. Part C: Journal of Mech. Eng. Sci. **230**, 2345 (2016).

[2] Xin Ning, Xueju Wang, Yi Zhang, Xinge Yu, Dongwhi Choi, Ning Zheng, Dong Sung Kim, Yonggang Huang, Yihui Zhang, and John A. Rogers, Assembly of advanced materials into 3d functional structures by methods inspired by origami and kirigami: A review, Adv. Mater. Interfaces **5**, 1800284 (2018).

[3] Jung Jae Park, Phillip Won, and Seung Hwan Ko, A review on hierarchical origami and kirigami structure for engineering applications, Int. J. Precision Eng. Manuf.-Green Technol. **6**, 147 (2019).

[4] Jon H. Myer and Frank Cooke, Optigami—a tool for optical systems design∗, Appl. Opt. **8**, 260 (1969).

[5] Sebastien J. P. Callens and Amir A. Zadpoor, From flat sheets to curved geometries: Origami and kirigami approaches, Mater. Today **21**, 241 (2018).

[6] James S. Cybulski, James Clements, and Manu Prakash, Foldscope: Origami-based paper microscope, PLoS ONE **9**, e98781 (2014).

[7] Shannon A. Zirbel, Robert J. Lang, Mark W. Thomson, Deborah A. Sigel, Phillip E. Walkemeyer, Brian P. Trease, Spencer P. Magleby, and Larry L. Howell, Accommodating thickness in origami-based deployable arrays, J. Mech. Des. **135**, 111005 (2013).

[8] Mark Schenk, A. D. Viquerat, K. A. Seffen, and S. D. Guest, Review of inflatable booms for deployable space structures: Packing and rigidization, J. Spacecraft Rockets **51**, 762 (2014).

[9] Yutaka Nishiyama, Miura folding: Applying origami to space exploration, Int. J. Pure Appl. Math. **79**, 269 (2012).

[10] Ivan Favero and Florian Marquardt, Focus on optomechanics, New J. Phys. **16**, 085006 (2014).

[11] C. Doolin, P. H. Kim, B. D. Hauer, A. J. R. MacDonald, and J. P. Davis, Multidimensional optomechanical cantilevers for high-frequency force sensing, New J. Phys. **16**, 035001 (2014).

[12] Houxun Miao, Kartik Srinivasan, and Vladimir Aksyuk, A microelectromechanically controlled cavity optomechanical sensing system, New J. Phys. **14**, 075015 (2012).

[13] Michael Schmidt, Max Ludwig, and Florian Marquardt, Optomechanical circuits for nanomechanical continuous variable quantum state processing, New J. Phys. **14**, 125005 (2012).

[14] S. J. M. Habraken, K. Stannigel, M. D. Lukin, P. Zoller, and P. Rabl, Continuous mode cooling and phonon routers for phononic quantum networks, New J. Phys. **14**, 115004 (2012).

[15] Masaaki Hashimoto and Yoshihiro Taguchi, Circular pyramidal kirigami microscanner with millimeter-range low-power lens drive, Opt. Express **28**, 17457 (2020).

[16] Yu Han, Zhiguang Liu, Shanshan Chen, Juan Liu, Yongtian Wang, and Jiafang Li, Cascaded multilayer nano-kirigami for extensible 3d nanofabrication and visible light manipulation, Photon. Res. **8**, 1506 (2020).

[17] Shanshan Chen, Wei Wei, Zhiguang Liu, Xing Liu, Shuai Feng, Honglian Guo, and Jiafang Li, Reconfigurable nano-kirigami metasurfaces by pneumatic pressure, Photon. Res. **8**, 1177 (2020).

[18] P.-Y. Madec, in *Adaptive Optics Systems III*, edited by Brent L. Ellerbroek, Enrico Marchetti, and Jean-Pierre Véran, International Society for Optics and Photonics (SPIE, 2012), Vol. 8447, p. 22.

[19] The LUVOIR Team, The LUVOIR Mission Concept Study Final Report, arXiv:1912.06219 [astro-ph.IM] (2019).

[20] Robert Huisman, Marcel P. Bruijn, Silvia Damerio, Martin J. Eggens, Syed Naveed R. Kazmi, Anja E. M. Schmerbauch, Heino P. Smit, Marco A. Vasquez-Beltran, Ewout Van der Veer, Mónica Acuautla, Bayu Jayawardhana, and Beatriz Noheda, High pixel number deformable mirror concept utilizing piezoelectric hysteresis for stable shape configurations, J. Astron. Telescopes, Instrum. Syst. **7**, 1 (2021).

[21] Laura Coyle, Scott Knight, Allison Barto, and Cody Allard, Ultra-stable telescope research and analysis (ultra) program - phase 1 report, NASA Contract 80NSSC18K0820 (2019).

[22] John W. Hardy, *Adaptive Optics for Astronomical Telescopes*, Oxford Series in Optical and Imaging Sciences (Oxford University Press, New York, 1998), p. 448.

[23] Takuso Sato, Hiroyuki Ishida, and Osamu Ikeda, Adaptive PVDF piezoelectric deformable mirror system, Appl. Opt. **19**, 1430 (1980).

[24] Krystian L. Wlodarczyk, Emma Bryce, Noah Schwartz, Mel Strachan, David Hutson, Robert R. J. Maier, David Atkinson, Steven Beard, Tom Baillie, Phil Parr-Burman, Katherine Kirk, and Duncan P. Hand, Scalable stacked array piezoelectric deformable mirror for astronomy and laser processing applications, Rev. Sci. Instrum. **85**, 024502 (2014).

[25] S. A. Cornelissen, A. L. Hartzell, J. B. Stewart, T. G. Bifano, and P. A. Bierden, in *Adaptive Optics Systems II*, edited by Brent L. Ellerbroek, Michael Hart, Norbert Hubin, and Peter L. Wizinowich, International Society for Optics and Photonics (SPIE, 2010), Vol. 7736, p. 898.

[26] Gleb Vdovin and Mikhail Loktev, Deformable mirror with thermal actuators, Opt. Lett. **27**, 677 (2002).

[27] Lei Huang, Xingkun Ma, Mali Gong, and Qi Bian, Experimental investigation of the deformable mirror with bidirectional thermal actuators, Opt. Express **23**, 17520 (2015).

[28] R. G. Gilbertson and J. D. Busch, A survey of micro-actuator technologies for future spacecraft missions, J. Br. Interplanetary Soc. **49**, 129 (1996).

[29] Roberto Biasi, Daniele Gallieni, Piero Salinari, Armando Riccardi, and Paolo Mantegazza, in *Adaptive Optics Systems II*, edited by Brent L. Ellerbroek, Michael Hart, Norbert Hubin, and Peter L. Wizinowich, International Society for Optics and Photonics (SPIE, 2010), Vol. 7736, p. 872.

[30] Shuyuan Xiao, Tao Wang, Tingting Liu, Chaobiao Zhou, Xiaoyun Jiang, and Jianfa Zhang, Active metamaterials and metadevices: A review, J. Phys. D: Appl. Phys. **53**, 503002 (2020).

[31] M. Miniaci, A. S. Gliozzi, B. Morvan, A. Krushynska, F. Bosia, M. Scalerandi, and N. M. Pugno, Proof of Concept for an Ultrasensitive Technique to Detect and Localize Sources of Elastic Nonlinearity Using Phononic Crystals, Phys. Rev. Lett. **118**, 214301 (2017).

[32] Marco Miniaci, Anastasiia Krushynska, Antonio S. Gliozzi, Nesrine Kherraz, Federico Bosia, and Nicola M. Pugno, Design and Fabrication of Bioinspired Hierarchical Dissipative Elastic Metamaterials, Phys. Rev. Appl. **10**, 024012 (2018).

[33] Ning An, August G. Domel, Jinxiong Zhou, Ahmad Rafsanjani, and Katia Bertoldi, Programmable hierarchical kirigami, Adv. Funct. Mater. **30**, 1906711 (2020).

[34] Yichao Tang, Gaojian Lin, Shu Yang, Yun Kyu Yi, Randall D. Kamien, and Jie Yin, Programmable kiri-kirigami metamaterials, Adv. Mater. **29**, 1604262 (2017).

[35] Doh-Gyu Hwang and Michael D. Bartlett, Tunable mechanical metamaterials through hybrid kirigami structures, Sci. Rep. **8**, 3378 (2018).

[36] Wei Zheng, Weicheng Huang, Feng Gao, Huihui Yang, Mingjin Dai, Guangbo Liu, Bin Yang, Jia Zhang, Yong Qing Fu, Xiaoshuang Chen, Yunfeng Qiu, Dechang Jia, Yu Zhou, and PingAn Hu, Kirigami-inspired highly stretchable nanoscale devices using multidimensional deformation of monolayer MoS2, Chem. Mater. **30**, 6063 (2018).

[37] Marcelo A. Dias, Michael P. McCarron, Daniel Rayneau-Kirkhope, Paul Z. Hanakata, David K. Campbell, Harold S. Park, and Douglas P. Holmes, Kirigami actuators, Soft Matter **13**, 9087 (2017).

[38] Yi Yang, Marcelo A. Dias, and Douglas P. Holmes, Multistable kirigami for tunable architected materials, Phys. Rev. Mater. **2**, 110601(R) (2018).

[39] See Supplemental Material at http://link.aps.org/supplemental/10.1103/PhysRevApplied.17.044012 for videos showing the proof-of-concept experiments of a sample with double and triple liftoff.

[40] Vasudevan Lakshminarayanan and Andre Fleck, Zernike polynomials: A guide, J. Mod. Opt. **58**, 545 (2011).

[41] E. Scott Claflin and Noah Bareket, Configuring an electrostatic membrane mirror by least-squares fitting with analytically derived influence functions, J. Opt. Soc. Am. A **3**, 1833 (1986).

[42] MATLAB, *version 9.6.0.1072779 (R2019a)* (The MathWorks Inc., Natick, Massachusetts, 2019).

[43] T. Bifano, MEMS deformable mirrors, Nat. Photonics **5**, 21 (2011).

[44] Allan Wirth, Jeffrey Cavaco, Theresa Bruno, and Kevin M. Ezzo, in *High-Power, High-Energy, and High-Intensity Laser Technology; and Research Using Extreme Light: Entering New Frontiers with Petawatt-Class Lasers*, edited by Georg Korn, Luis Oliveira Silva, and Joachim Hein, International Society for Optics and Photonics (SPIE, 2013), Vol. 8780, p. 122.

[45] Corentin Coulais, Eial Teomy, Koen de Reus, Yair Shokef, and Martin van Hecke, Combinatorial design of textured mechanical metamaterials, Nature **535**, 529 (2016).